

Spin diffusion/transport in n -type GaAs quantum wells

J. L. Cheng and M. W. Wu*

*Hefei National Laboratory for Physical Sciences at Microscale,
University of Science and Technology of China, Hefei, Anhui, 230026, China and*

Department of Physics, University of Science and Technology of China, Hefei, Anhui, 230026, China[†]
(Dated: September 29, 2018)

The spin diffusion/transport in n -type (001) GaAs quantum well at high temperatures (≥ 120 K) is studied by setting up and numerically solving the kinetic spin Bloch equations together with the Poisson equation self-consistently. All the scattering, especially the electron-electron Coulomb scattering, is explicitly included and solved in the theory. This enables us to study the system far away from the equilibrium, such as the hot-electron effect induced by the external electric field parallel to the quantum well. We find that the spin polarization/coherence oscillates along the transport direction even when there is no external magnetic field. We show that when the scattering is strong enough, electron spins with different momenta oscillate in the same phase which leads to equal transversal spin injection length and ensemble transversal injection length. It is also shown that the intrinsic scattering is already strong enough for such a phenomena. The oscillation period is almost independent on the external electric field which is in agreement with the latest experiment in bulk system at very low temperature [Europhys. Lett. **75**, 597 (2006)]. The spin relaxation/dephasing along the diffusion/transport can be well understood by the inhomogeneous broadening, which is caused by the momentum-dependent diffusion and the spin-orbit coupling, and the scattering. The scattering, temperature, quantum well width and external magnetic/electric field dependence of the spin diffusion is studied in detail.

PACS numbers: 72.25.Rb, 72.25.Dc, 72.20.Ht, 67.57.Lm

I. INTRODUCTION

The study of semiconductor spintronics¹ has caused a lot of attention since long spin lifetime and large spin transport distance have been observed in n -type semiconductors,^{2,3,4,5,6,7,8} due to the great potential of the device applications such as quantum memory devices, spin valves and spin transistors. High spin injection efficiency and long spin diffusion/transport distance are two prerequisites of realizing these devices and have been widely studied both experimentally^{9,10,11,12,13,14,15,16} and theoretically.^{17,18,19,20,21,22,23,24,25,26,27,28,29,30,31,32,33,34,35} Many works are focused on improving the spin injection efficiency by electrical method.^{12,13,14,30,36,37} Others are concentrated on the spin diffusion/transport inside the semiconductors without taking care of the injection.^{15,16,20,21,23,24,25,26,28,32,33} In the latter case, the spin polarization can be prepared by optical excitations.^{15,16,38} A number of theories have been developed to study the spin transport, such as the two-component drift-diffusion model,^{20,22,23,24} the kinetic spin Bloch equation approach,^{21,25,27,28,32} the Monte-Carlo simulation,^{29,30,31,33,40} and the microscopic semiclassical approach.^{41,42,43,44} In these theories, Weng and Wu showed that the correlations between the spin-up and -down states, *i.e.*, the off-diagonal terms of the density matrix in spin space, play an essential role in spin diffusion/transport.²¹ By constructing the kinetic spin Bloch equations by means of the non-equilibrium Green function method and numerically solving these equations with the scattering explicitly included, they predicted

spin oscillations along the spin diffusion in the absence of the magnetic field^{25,27} which cannot be obtained from the two-component drift-diffusion model. These oscillations were later observed in experiments.^{15,16} Now most of the theoretical works include the off-diagonal terms.^{16,21,25,26,27,28,29,32,33,41}

Another important consequence of the off-diagonal terms is that they allow spin to precess along the effective magnetic field which originates from the spin-orbit coupling (SOC) and is momentum dependent. The fact that spin with different momentum precesses with different frequency is referred to as inhomogeneous broadening.^{45,51} It was shown by Wu *et al.* in the spacial uniform systems that in the presence of the inhomogeneous broadening, any spin conserving scattering, including the Coulomb scattering, can cause irreversible spin relaxation/dephasing (R/D).^{45,46,47,48,49,50} Later Weng and Wu extended this concept to the spacial inhomogeneous systems and showed that the spin with different momentum precesses with different frequencies during the diffusion along the spacial gradient, thanks to the off-diagonal term.²¹ This serves as additional inhomogeneous broadening and can cause additional spin R/D combined with the spin conserving scattering.^{21,25,28}

In our previous works, we have studied both the transient^{25,28} and the steady-state^{21,25,27} spin diffusion/transport in GaAs quantum well (QW) using the kinetic spin Bloch equations, first without^{21,25} and then with^{27,28} the Coulomb scattering. The other scattering such as electron-phonon and electron-impurity scattering is explicitly included. By solving the kinetic spin Bloch

equations combined with the Poisson equation, one is able to obtain the mobility, diffusion length and spin injection length without any fitting parameter. Moreover, this approach is valid not only for systems near the equilibrium, but also for those far away from the equilibrium such as systems under strong external electric field (hot-electron effect) and/or with large spin polarization. It is also applicable to systems in both the strong scattering regime and the weak one.⁵⁰ Nevertheless, in our previous investigation of the steady-state spin transport,^{21,25} the boundary conditions we used are the single-side ones, *i.e.*, $\rho_{k_x\sigma\sigma'}(x=0)$ are given from the single side of the sample regardless of the sign of k_x , with $\rho_{k_x\sigma\sigma'}(x)$ representing the density matrix elements. This is an approximation as in principal $\rho_{k_x\sigma\sigma'}(x=0)$ for $k_x < 0$ ($k_x > 0$) can only be determined from the right (left) side of $x=0$. Moreover, by using this boundary conditions, the grid of the space has to be very small due to the reason specified in the next section. Therefore the length of the sample we studied before is very short, even less than one oscillation period, as the numerical calculation is too time-consuming.^{21,25} It is therefore also almost impossible to discuss situations such as spin transport under strong external electric fields. In this paper, we adopt the double-side boundary conditions which are widely used in the charge transport,^{52,53,54} *i.e.*, using $\rho_{k_x\sigma\sigma'}(x=0)$ and $\rho_{-k_x\sigma\sigma'}(x=L)$ as boundary conditions with $k_x > 0$ and L standing for the right side of the sample. We further develop new numerical scheme to solve the kinetic equations with all the scattering included. This allows us to solve the spin diffusion/transport with fast speed and high accuracy. We therefore study the spin diffusion/transport with large sample scale under various conditions such as temperature, well width, magnetic field and electric field. The hot-electron effect to the spin transport is also discussed in detail.

This paper is organized as follows: In Sec. II we set up the model and construct the kinetic spin Bloch equations with the boundary conditions by using the Keldysh Green function method. In Sec. III we present our main results of the spin diffusion/transport with different scattering, temperature, quantum well width, external magnetic field and external electric field. We conclude in Sec. IV. In Appendix A we give the scheme for the numerical calculation.

II. MODEL AND KINETIC SPIN BLOCH EQUATIONS

We begin our study from a two dimensional electron gas (2DEG) confined by an infinite square well with width a along the (001) direction. The growth direction is assumed to be along the z -axis. A moderate magnetic field B and an electric field E are applied along the x - y plane with the x -axis being the diffusion/transport direction. The electron state is described by a subband index n which comes from the confinement of the QW,

a 2D momentum $\mathbf{k} = (k_x, k_y)$, which represents the momentum along the x - y -plane and the spin index σ , which stands for the spin-up (\uparrow) or -down (\downarrow) state along the z -axis. In the present paper, the width of the QW is taken to be so small that only the lowest subband $n=1$ is occupied and the higher subbands are negligible.

By using the nonequilibrium Green function method with the gradient expression as well as the generalized Kadanoff-Baym ansatz,⁵⁵ we construct the kinetic spin Bloch equations as follows^{21,25}

$$\frac{\partial}{\partial t}\rho_{\mathbf{k}}(\mathbf{r}, t) = \left. \frac{\partial}{\partial t}\rho_{\mathbf{k}}(\mathbf{r}, t) \right|_{\text{dr}} + \left. \frac{\partial}{\partial t}\rho_{\mathbf{k}}(\mathbf{r}, t) \right|_{\text{dif}} + \left. \frac{\partial}{\partial t}\rho_{\mathbf{k}}(\mathbf{r}, t) \right|_{\text{coh}} + \left. \frac{\partial}{\partial t}\rho_{\mathbf{k}}(\mathbf{r}, t) \right|_{\text{scat}}. \quad (1)$$

Here $\rho_{\mathbf{k}}(\mathbf{r}, t) = \begin{pmatrix} f_{\mathbf{k}\uparrow} & \rho_{\mathbf{k}\uparrow\downarrow} \\ \rho_{\mathbf{k}\downarrow\uparrow} & f_{\mathbf{k}\downarrow} \end{pmatrix}$ are the density matrices of electrons with momentum \mathbf{k} at position $\mathbf{r} = (x, y)$ and time t . The diagonal elements $f_{\mathbf{k},\sigma}$ stand for the electron distribution functions of spin σ whereas the off-diagonal elements $\rho_{\mathbf{k}\uparrow\downarrow} = \rho_{\mathbf{k}\downarrow\uparrow}^* \equiv \rho_{\mathbf{k}}$ represent the correlations between the spin-up and -down states.

$$\left. \frac{\partial \rho_{\mathbf{k}}(\mathbf{r}, t)}{\partial t} \right|_{\text{dr}} = \frac{1}{2} \{ \nabla_{\mathbf{r}} \bar{\epsilon}_{\mathbf{k}}(\mathbf{r}, t), \nabla_{\mathbf{k}} \rho_{\mathbf{k}}(\mathbf{r}, t) \} \quad (2)$$

are the driving terms from the external electric field. Here

$$\bar{\epsilon}_{\mathbf{k}}(\mathbf{r}, t) = \frac{\mathbf{k}^2}{2m^*} + [g\mu_B \mathbf{B} + \mathbf{h}(\mathbf{k})] \cdot \frac{\boldsymbol{\sigma}}{2} - e\Psi(\mathbf{r}) + \mathcal{E}_{\text{HF}}(\mathbf{r}, t) \quad (3)$$

with m^* denoting the effective mass. $\mathbf{h}(\mathbf{k})$ is the D'yakonov and Perel' (DP)⁵⁶ effective magnetic field from the Dresselhaus⁵⁷ and the Rashba⁵⁸ terms. For GaAs, the Dresselhaus term is the leading term and $\mathbf{h}(\mathbf{k})$ reads

$$\mathbf{h}(\mathbf{k}) = (\gamma k_x(k_y^2 - \langle k_z^2 \rangle), \gamma k_y(\langle k_z^2 \rangle - k_x^2), 0). \quad (4)$$

Here the spin splitting parameter γ is given by³⁸

$$\gamma = (4/3)(m^*/m_{cv})(1/\sqrt{2m^*E_g})(\eta/\sqrt{1-\eta/3}), \quad (5)$$

in which $\eta = \Delta/(E_g + \Delta)$; E_g denotes the band gap; Δ represents the spin-orbit splitting of the valence band; m^* standing for the electron mass in GaAs; and m_{cv} is a constant close in magnitude to the free electron mass m_0 .³⁹ For GaAs $\gamma_0 = 11.4 \text{ eV} \cdot \text{\AA}^3$. $\langle k_z^2 \rangle$ stands for the average of the operator $-(\partial/\partial z)^2$ over the electronic state of the lowest subband and being $(\pi/a)^2$ under the infinite-well-depth assumption. $\mathcal{E}_{\text{HF}}(\mathbf{r}, t) = -\sum_{\mathbf{q}} V_{\mathbf{q}} \rho_{\mathbf{k}-\mathbf{q}}(\mathbf{r}, t)$ is the Hartree-Fock term, *i.e.* the exchange term,⁵⁵ with $V_{\mathbf{q}} = \sum_{q_z} \frac{4\pi e^2}{\kappa_0(\mathbf{q}^2 + q_z^2 + \kappa^2)} |I(iq_z)|^2$ the screened coulomb potential and $\kappa^2 = 4\pi e^2 n_0 / (ak_B T)$ the Debye-Hückel screening constant. Here κ_0 is the static dielectric constant, n_0 represents the 2D electron density

and $|I(iq_z)|^2 = \pi^4 \sin^2 y / [y^2(y^2 - \pi^2)^2]$ is the form factor with $y = q_z a / 2$. The Hartree-Fock term is important only when there is a large spin polarization.⁴⁷ For the small spin polarization explored in this paper, it can be ignored. $\Psi(\mathbf{r})$ is the electric potential which satisfies the Poisson equation:⁵⁹

$$\nabla_{\mathbf{r}}^2 \Psi(\mathbf{r}) = e[n(\mathbf{r}) - N_0(\mathbf{r})] / (a\kappa_0) \quad (6)$$

with $n(\mathbf{r})$ standing for the electron density at position \mathbf{r} and $N_0(\mathbf{r})$ representing the background positive charge density. The bracket $\{A, B\} = AB + BA$ in Eq. (2) is the anti-commutator.

$$\left. \frac{\partial \rho_{\mathbf{k}}(\mathbf{r}, t)}{\partial t} \right|_{\text{dif}} = -\frac{1}{2} \{ \nabla_{\mathbf{k}} \bar{\varepsilon}_{\mathbf{k}}(\mathbf{r}, t), \nabla_{\mathbf{r}} \rho_{\mathbf{k}}(\mathbf{r}, t) \} \quad (7)$$

are the diffusion terms which also give the additional inhomogeneous broadening due to the broadening of the spin precession frequencies for different momentum \mathbf{k} along the spacial gradient.²¹ The coherent terms $\left. \frac{\partial \rho_{\mathbf{k}}(\mathbf{r}, t)}{\partial t} \right|_{\text{coh}}$ and the scattering terms $\left. \frac{\partial \rho_{\mathbf{k}}(\mathbf{r}, t)}{\partial t} \right|_{\text{scat}}$ can be found in Refs. 48 and 60.

In the present paper it is assumed that a spin polarization is injected from the left side of the sample and diffuse/transport along the x -axis. Its spacial distribution along the y -axis is uniform. The kinetic spin Bloch equations are then simplified into

$$\frac{\partial \rho_{\mathbf{k}}(x, t)}{\partial t} + e \frac{\partial \Psi(x, t)}{\partial x} \frac{\partial \rho_{\mathbf{k}}(x, t)}{\partial k_x} + \frac{k_x}{m^*} \frac{\partial \rho_{\mathbf{k}}(x, t)}{\partial x} + i \left[(g\mu_B \mathbf{B} + \mathbf{h}(\mathbf{k})) \cdot \frac{\boldsymbol{\sigma}}{2}, \rho_{\mathbf{k}}(x, t) \right] = \left. \frac{\partial \rho_{\mathbf{k}}(x, t)}{\partial t} \right|_{\text{scat}}. \quad (8)$$

Here the spin-orbit coupling $\partial \mathbf{h}(\mathbf{k}) / \partial k_x \cdot \boldsymbol{\sigma} / 2$ in the diffusion term is very small in comparison to k_x / m^* and is ignored. The inhomogeneous broadening can be easily seen from these equations. For the spacial uniform case, $\partial \rho_{\mathbf{k}}(x, t) / \partial x = 0$ and the electron spin precession is inhomogeneously broadened only due to the momentum-dependent effective magnetic field $\mathbf{B}_e(\mathbf{k}) \equiv \mathbf{h}(\mathbf{k}) / g\mu_B + \mathbf{B}$. With this inhomogeneous broadening, spin conserving scattering including the Coulomb scattering^{21,45,50,61} results in an irreversible spin R/D. Moreover, the scattering can also give a counter effect to the inhomogeneous broadening.⁵⁰ It is noted that unless the g -factor is inhomogeneously broadened,^{45,62} the external magnetic field itself cannot cause any inhomogeneous broadening. So there is no spin R/D when $\mathbf{h}(\mathbf{k}) = 0$.⁴⁵ For the spacial inhomogeneous case, besides the spin precession around the effective magnetic field, its diffusion into the semiconductor also accompanies a spin precession with the precession frequency being \mathbf{k} -dependent, *i.e.*, the third term in Eq. (8). So this causes additional inhomogeneous broadening. Moreover, in the steady-state spin diffusion/transport, the spin precession rate along the diffusion direction is determined by $|g\mu_B \mathbf{B} + \mathbf{h}(\mathbf{k})| / k_x$ according to Eq. (8). Therefore, differing from the spacial uniform case, the external magnetic field itself *alone*

can cause spin R/D along the diffusion direction due to the inhomogeneous broadening of the diffusion velocity k_x / m^* .²¹

The kinetic spin Bloch equations (8) together with the Poisson equation (6) are highly nonlinear and have to be solved numerically. In our previous paper,²⁵ this set of equations are solved with single-side boundary conditions. In such a method, an extra parameter, so called the coefficient of viscosity,⁵² is introduced to keep the smoothness of the solution and the Poisson equation is inevitable to keep the system from divergence even though there are no charge imbalance and external electric field. This can be seen by retaining the third terms in Eq. (8) and replacing the scattering terms by the relaxation time approximation:

$$\frac{k_x}{m^*} \frac{\partial \rho_{\mathbf{k}}(x)}{\partial x} = -\frac{\rho_{\mathbf{k}}(x) - \rho_{\mathbf{k}}^0}{\tau_p}, \quad (9)$$

with $\rho_{\mathbf{k}}^0$ representing the density matrices in the equilibrium. It is clearly seen from this equation that $\rho_{\mathbf{k}}(x)$ is divergent when $x \rightarrow \infty$ for $k_x < 0$. In order to circumvent this divergence, the Poisson equation has to be applied and the grid for the space has to be very small. In the present investigation we extend the conventional numerical scheme of solving the Boltzmann equation for charge transport^{52,53} to solve the kinetic spin Bloch equations by using the double-side boundary conditions. This conditions assume a finite sample length L and are given by

$$\begin{cases} \rho_{\mathbf{k}}(x=0, t) = F(\varepsilon_{\mathbf{k},E} - \mu(0)) , & \text{for } k_x > 0 , \\ \rho_{\mathbf{k}}(x=L, t) = F(\varepsilon_{\mathbf{k},E} - \mu(L)) , & \text{for } k_x < 0 . \end{cases} \quad (10)$$

Here $F(\varepsilon_{\mathbf{k},E} - \mu(x)) \equiv [\exp(\varepsilon_{\mathbf{k},E} - \mu(x)) / (k_B T_e) + 1]^{-1}$ represent the drifted Fermi distributions in the spin space,

with the chemical potential matrices $\mu(0) = \begin{pmatrix} \mu_{\uparrow} & 0 \\ 0 & \mu_{\downarrow} \end{pmatrix}$

and $\mu(L) = \begin{pmatrix} \mu_0 & 0 \\ 0 & \mu_0 \end{pmatrix}$ if the spin injection is from the left side and L is assumed to be large enough so that the spin polarization vanishes before it reaches the right boundary. $\varepsilon_{\mathbf{k},E} = (\mathbf{k} - m^* \mu_E \mathbf{E})^2 / 2m^*$ is energy spectrum drifted by the electric field. T_e and μ_E are the hot electron temperature and mobility respectively which are calculated at the spacial uniform case following the method addressed in our previous paper.⁴⁸ The initial electron distributions are given by

$$\rho_{\mathbf{k}}(x, t=0) = F(\varepsilon_{\mathbf{k},E} - \mu(x)) , \quad (11)$$

with $\mu(0) = \begin{pmatrix} \mu_{\uparrow} & 0 \\ 0 & \mu_{\downarrow} \end{pmatrix}$ and $\mu(x \neq 0) = \begin{pmatrix} \mu_0 & 0 \\ 0 & \mu_0 \end{pmatrix}$. The chemical potentials $\mu_{\uparrow(\downarrow)}$ and μ_0 are determined by the equations

$$\sum_{\mathbf{k}} \text{Tr}[\rho_{\mathbf{k}}(x, 0)] = n(x) , \quad (12)$$

$$\sum_{\mathbf{k}} \text{Tr}[\rho_{\mathbf{k}}(0, 0) \sigma_z] = Pn(0) , \quad (13)$$

with P denoting the spin polarization at the boundary $x = 0$. The double-side boundary conditions are in good consistence with the physical consideration that the electron must move along its momentum direction. For the Poisson equation, its boundary conditions are set to be $\Psi(0) = 0$ and $\Psi(L) = EL$ with E representing the strength of the external electric field. The numerical scheme for the scattering terms has been laid out in detail in our previous paper⁴⁸ and the new numerical scheme for solving the kinetic spin Bloch equations is given in Appendix A. By using this new scheme, we further remove the extra parameter—the coefficient of viscosity.

III. NUMERICAL RESULTS

We numerically solve the kinetic spin Bloch equations (8) together with the Poisson equation (6) iteratively to achieve the self-consistent solution. We include all the scattering, *i.e.*, the electron-electron Coulomb, the electron-phonon and the electron-impurity scattering. As we are interested in the diffusion/transport properties at high temperatures ($T \geq 120$ K), for the electron-phonon scattering we only need to consider the electron-longitudinal-optical (LO) phonon scattering.^{65,66,67} All matrix elements of the interactions and the expressions of the scattering terms can be found in Ref. 48. The width of the QW and the electron density are taken to be $a = 7.5$ nm and $N_e = 4 \times 10^{11}$ cm⁻² separately unless otherwise specified. The initial spin polarization of the left boundary is $P = 5\%$. In the numerical calculation, we divide the momentum \mathbf{k} -space into $N \times M$ control regions as plotted in Fig. 8 in Ref. 48 and the corresponding center points are

$$\mathbf{k}_{n,m} = \sqrt{(n + \frac{1}{2})\Delta E} \left(\sin \frac{2m\pi}{M}, \cos \frac{2m\pi}{M} \right) \quad (14)$$

with $n = 0, \dots, N - 1$ and $m = 0, \dots, M - 1$. In the present work, we take $(N, M) = (16, 18)$.⁶⁸ The energy cut is determined by the ratio between the distribution at the energy cut and the distribution at the zero energy is less than 0.1 %, which is around $10E_f$ at $T = 200$ K with $E_f = 14.3$ meV being the Fermi energy. The sample length is usually taken to be $L = 10$ μ m, unless otherwise specified. This length has to be taken long enough so that the spin polarization effectively vanishes at the right boundary. The other parameters are listed in Table I.⁶⁹

κ_0	10.8	κ_∞	12.9
Ω_{LO}	35.4 meV	m^*	$0.067m_0$
g	0.44	E_g	1.55 eV
α_0	5.33 Å	Δ	0.341 eV

TABLE I: Parameters used in the numerical calculations, Ω_{LO} is the LO phonon energy.

Three quantities are used to describe the spin diffusion/transport lengths in the steady state: spin-dependent electron density

$$N_\sigma(x) = \sum_{\mathbf{k}} f_{\mathbf{k},\sigma}(x), \quad (15)$$

the incoherently summed spin coherence

$$\rho(x) = \sum_{\mathbf{k}} |\rho_{\mathbf{k}\uparrow\downarrow}(x)|, \quad (16)$$

and the coherently summed spin coherence

$$\rho'(x) = \left| \sum_{\mathbf{k}} \rho_{\mathbf{k}\uparrow\downarrow}(x) \right|. \quad (17)$$

Unlike the corresponding quantities defined in the time domain,⁷⁰ these three quantities are defined in the spacial domain. The irreversible spin dephasing length L_p can be deduced from the decay of the envelope of ρ ;^{21,63,64} the ensemble spin diffusion length L_p^* is given by the decay of the envelope of ρ' ; whereas the spin diffusion length L_d is determined from the decay of the envelope of $\Delta N = N_\uparrow - N_\downarrow$.

A. Transient momentum-resolved spacial evolution of spin polarization

We first show the spacial dependence of $f_{\mathbf{k},\sigma}$ for different momentums \mathbf{k} at $t = 5, 10$ and 300 ps in Fig. 1(a) with the electron-electron and the electron-LO-phonon scattering included. $T = 200$ K and $B = 0$. Differing from the intuition that the spin precession should be controlled by the effective magnetic field $\mathbf{h}(\mathbf{k})$, it is seen from the figure that the electron spins with different momentums present almost the identical precession period. This is understood due to the strong scattering which enforces different spins to precess with the same frequency. In order to reveal this effect, we scale all the scattering terms with a scaling factor λ , *i.e.*, replacing the scattering terms in Eq. (8) by $\lambda \frac{\partial \rho_{\mathbf{k}}(x,t)}{\partial t}|_{\text{scat}}$. First we consider the case without any scattering and electric field, *i.e.*, $\lambda = 0$ and $\mathbf{E} = \nabla_{\mathbf{r}}\Psi(\mathbf{r}) = 0$. It is then easy to obtain the analytical solution of Eq. (8) in the steady state with the boundary conditions (10):

$$\rho_{\mathbf{k}}(x) = \begin{cases} e^{-\frac{im^*}{2k_x} g\mu_B \mathbf{B}_e(\mathbf{k}) \cdot \boldsymbol{\sigma}_x} \rho_{\mathbf{k}}(x=0) e^{\frac{im^*}{2k_x} g\mu_B \mathbf{B}_e(\mathbf{k}) \cdot \boldsymbol{\sigma}_x}, & k_x > 0 \\ \rho_{\mathbf{k}}(x=L), & k_x < 0 \end{cases} \quad (18)$$

by further neglecting the HF terms. This solution is somehow different from our previous analytical result²⁵ due to the different boundary conditions. It describes the injection of the electron spin with momentum \mathbf{k} from both boundaries into the 2DEG. For each electron with $k_x < 0$, it comes from the right boundary ($x = L$) where there is no spin polarization. So there is no spin precession in the 2DEG. However, for electron with $k_x > 0$, it comes from the left boundary where the electron spin is polarized. The spin polarization precesses in the 2DEG due to the presence of the effective magnetic field $\mathbf{B}_e(\mathbf{k})$. Moreover it does not decay in the absence of any scattering. It is noted from Eq. (18) that unlike the temporal spin precession where the precession rate is determined by $g\mu_B |\mathbf{B}_e(\mathbf{k})|$, the spacial spin precession rate is determined by

$$\Omega_{\mathbf{k}} = m^* g\mu_B \mathbf{B}_e(\mathbf{k}) / k_x \quad (19)$$

which strongly depends on the velocity k_x/m^* . This is because in Eq. (8) the diffusion term is proportional to the velocity. This gives strong inhomogeneous broadening along the spin diffusion.²¹

Then we introduce the scattering into the system, first a small one with $\lambda = 0.05$ [Fig. 1(c)] and then the normal one with $\lambda = 1$ [Fig. 1(a)], which are compared with the case with $\lambda = 0$ [Fig. 1(b)]. Once the scattering term is turned on, the electron spin presents a very different evolution behavior from Eq. (18). First, electrons with $k_x < 0$ [curves for different wavevector $\mathbf{k}_{n,m}$ (Eq. (14)) with $(n, m) = (0, 7)$ and $(5, 7)$] obtain a spin polarization due to the scattering which scatters electrons with $k_x > 0$ to those with $k_x < 0$ and hence the spin polarization is transferred from electrons with $k_x > 0$. Consequently this kind of spin polarization is also built up from the left edge to the right one even though $k_x < 0$. Second, the scattering tends to drive the spin precession and spin diffusion to reach the same precession frequency and diffusion velocity respectively for different \mathbf{k} . This can be seen from Fig. 1 where $\Delta f_{\mathbf{k}} = f_{\mathbf{k}\uparrow} - f_{\mathbf{k}\downarrow}$ is plotted against the position x for different momentum \mathbf{k} at $t = 5, 10$, and 300 ps (already in the steady state) by comparing the results with $\lambda = 0$ (no scattering), $\lambda = 0.05$ (weak scattering) and $\lambda = 1$ (normal scattering). In the computation we only include the electron-electron and electron-LO-phonon scattering. It is easy to find that when there is no/weak scattering, spin precession frequencies and spin diffusion velocities with different momentum show different values. However, when the scattering becomes stronger, the spacial spin precession frequencies and the spin diffusion velocities for different momentum \mathbf{k} tend to a single frequency and velocity as shown in Fig. 1(a).

The same behavior is also observed for the spin coherence $\rho_{\mathbf{k}\uparrow\downarrow}$ as shown in Fig. 1(d) in the steady state ($t = 300$ ps). This is also the reason that the numerical results are highly accurate even for small grid numbers in the \mathbf{k} -space. Moreover, it shows that when the scattering is strong enough, there is no interference-induced decay and consequently $L_p = L_p^*$. The similar results have been obtained in the time domain.⁷⁰ In fact, even for the case $N_e = 4 \times 10^{10} \text{ cm}^{-2}$ and $T = 120 \text{ K}$, the intrinsic scattering is already strong enough to ensure this behavior. Spin echo experiments are needed to verify our findings here.⁷¹

This behavior can be understood as following: Without the scattering, each spin precesses with its own frequency $\Omega_{\mathbf{k}}$ independently with the \mathbf{k} -dependent precession frequency referred to as the inhomogeneous broadening. Scattering tends to suppress this inhomogeneous broadening and to make it a homogeneous one. Our result indicates that the intrinsic scattering (the electron-electron and electron-phonon scattering) is already strong enough to totally suppress the inhomogeneous broadening. The spin polarizations for different \mathbf{k} all precess with single frequency $\langle \Omega_{\mathbf{k}} \rangle = \Omega_0 = m^* \gamma (\langle k_y^2 \rangle - \langle k_z^2 \rangle, 0, 0)$ when $B = 0$. In the case we calculate here, $\Omega_0 = -1.61/\mu\text{m}$ ($\gamma = 11.4 \text{ eV} \cdot \text{\AA}^3$, $\langle k_y^2 \rangle \approx \frac{1}{2} \frac{2m^*}{\hbar^2} k_B T$ for the non-degenerate case) which corresponds to the spacial period $3.88 \mu\text{m}$.

Moreover, it is seen from the figure that besides the counter effect of the scattering to the inhomogeneous broadening, it also causes irreversible spin R/D.⁴⁵ In the steady state, there is no spin relaxation for each \mathbf{k} , as shown in Fig. 1(b) in the absence of any scattering. Whereas strong spin relaxation is observed in Fig. 1(a) in the presence of unscaled intrinsic scattering.

Finally the scattering also affects the total spin polarization at the left boundary in the steady state. It is noted that the boundary conditions Eq. (10) at $x = 0$ are only for $k_x > 0$. The total spin polarization Eq. (13) is determined by the contributions from both $k_x > 0$ and $k_x < 0$. Without scattering, the spin polarization for $k_x < 0$ is always zero [Eq. (18) and Fig. 1(b)]. Therefore, the total spin polarization is only one half of 5 % at the left boundary. The scattering transfers spin polarization from states of $k_x > 0$. Therefore, the larger the scattering, the closer the total spin polarization approaches the boundary condition: $P = 3.0 \%$ for $\lambda = 0.05$ and 4.5% for $\lambda = 1.0$. We believe that the spin polarization at the left boundary can be very close to 5 % for sufficiently strong scattering. In such a case, the spin injection with double-side boundary conditions can be approximated by the single-side boundary conditions used

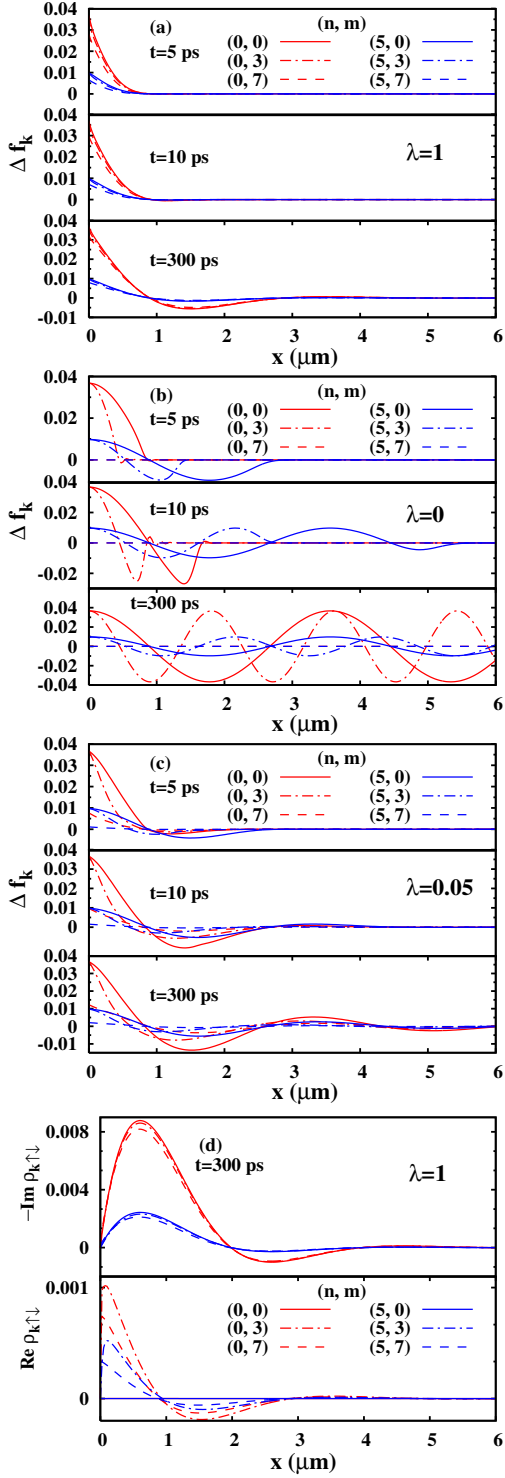


FIG. 1: (Color online) $\Delta f_{\mathbf{k}}$ [(a)-(c)] and $\rho_{\mathbf{k}\uparrow\downarrow}$ [(d)] vs. x for different $\mathbf{k}_{n,m}$ at $t = 5, 10$ and 300 ps (with the system being in the steady state at 300 ps). $T = 200$ K and $B = 0$. (b) no scattering: $\lambda = 0$; (c) small scattering: $\lambda = 0.05$; (a) and (d) normal scattering $\lambda = 1$. Only the electron-electron and the electron-LO phonon scattering is included in the calculation. It is noted that although x is plotted up to $6 \mu\text{m}$, the sample length L used in the calculation is $10 \mu\text{m}$.

in our previous papers.^{21,25} However, for small spin polarizations, the spin injection properties such as the spin diffusion length and the spin precession period are not determined by the initial spin polarization at the boundary.

B. Effect of scattering on spin diffusion

As shown in the previous subsection that the scattering plays a crucial role when the electron diffuse/transport into the 2DEG, we now study the effect of the scattering on the total spin signal. In Fig. 2 the spin-resolved electron density N_{σ} [Eq. (15)] and the incoherently summed spin coherence ρ [Eq. (17)] in the steady state are plotted against the position x by first including only the electron-LO-phonon scattering (red curves), then adding the electron-electron scattering (green curves) and finally adding the electron-impurity scattering (blue curves) with $N_i = N_e$ at $T = 120$ K (a) and 300 K (b). $B = 0$ in the calculation.

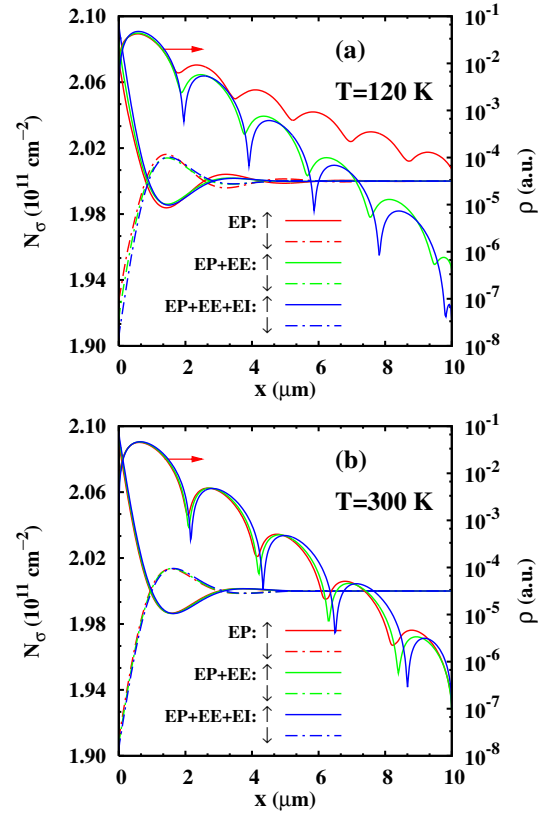


FIG. 2: (Color online) Effect of the scattering on spin diffusion in the steady state at (a) $T = 120$ K and (b) $T = 300$ K. Red curves: with only the electron-LO-phonon (EP) scattering; Green curves: with both the electron-electron (EE) and EP scattering; Blue curves: with all the scattering, *i.e.*, the EE, EP and electron-impurity (EI) scattering. The impurity density $N_i = N_e$. Note the scale of the incoherently summed spin coherence is on the right hand side of the figure.

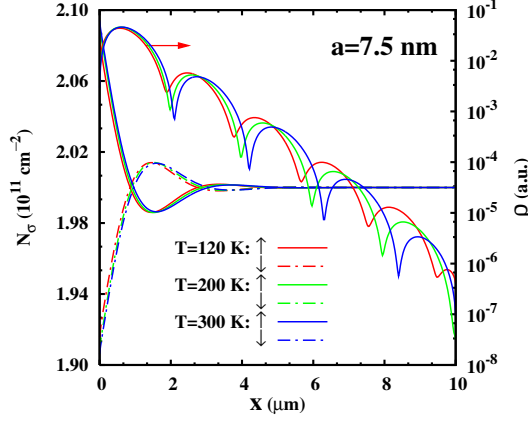


FIG. 3: (Color Online) N_σ and ρ vs. the position x at $T = 120, 200$ and 300 K with width $a = 7.5$ nm and $L = 10$ μm . $N_i = 0$. Note the scale of the incoherently summed spin coherence is on the right hand side of the figure.

It is seen from the figure that similar to the transient spin diffusion in our previous investigation,^{25,27,28} both N_σ and ρ oscillate with the position even when there is *no* external magnetic field here. Besides the oscillation, strong spin relaxation and dephasing are observed. Nevertheless, they present a more complicated behavior: When $T = 120$ K, the spin relaxation and dephasing always decrease when a new scattering is added. However, when $T = 300$ K, they become faster when the electron-electron scattering is added to the case with only the electron-LO-phonon scattering but become slower when electron-impurity scattering is further added. Finally, the spin polarizations at the left boundary are 4.75 %, 4.20 % and 3.60 % at 120 K and 4.8 %, 4.7 % and 4.6 % at 300 K for the cases with all the scattering, with both the electron-electron and the electron-LO-phonon scattering and with only the electron-LO-phonon scattering, respectively. *i.e.*, the spin polarization at the left boundary always increases with the strengthening of the scattering, either the strengthening is due to the addition of more scattering or due to the increase of temperature. This is consistent with the result in the previous subsection.

The spin precession in the steady-state spin injection in the absence of the magnetic field is in consistence with the latest experimental observation in bulk system.¹⁵ This kind of spacial precession is different from the spin precession in the time domain,¹¹ where the spin precession can also be observed in the absence of any magnetic field in 2DEG when $T < 2$ K. This is because the inhomogeneous broadening in the time domain is $\mathbf{h}(\mathbf{k})$ with its average over a homogenous electron distribution being $\langle \mathbf{h}(\mathbf{k}) \rangle = 0$, which is too weak to sustain the scattering when the temperature is higher than 2 K. However, the spin precession in the real space during the diffusion is quite different. Here the inhomogeneous broadening is caused by $\mathbf{\Omega}_\mathbf{k} = m^* \mathbf{h}(\mathbf{k})/k_x$ with $\langle \mathbf{\Omega}_\mathbf{k} \rangle = \mathbf{\Omega}_0 \neq 0$. From previous subsection, we know the precessions of different

wave vector \mathbf{k} share the same frequency Ω_0 even with the normal intrinsic scattering. So the total spin polarization oscillates in the space and this kind of oscillations exist even in the room temperature. However, in the experiments by Beck *et al.*,¹⁵ as $\langle k_y^2 \rangle = \langle k_z^2 \rangle$ in the bulk system, $\Omega_0 = 0$ and the effective magnetic field is provided by strain which is very small. This is the reason in bulk one has to observe the spin oscillations at very low temperature.

The complicated scattering dependence of the spin R/D in the real space is similar to that of the spin R/D in the time domain,^{49,50} where the scattering dependence of the spin R/D time is different in the strong and weak scattering regimes.⁵⁰ In the weak scattering limit, adding a new scattering increases the spin R/D as it provides more spin R/D channel in the presence of the inhomogeneous broadening. Nevertheless, in the strong scattering limit, the counter effect of the scattering to the inhomogeneous broadening is important and adding a new scattering leads to a weaker spin R/D.⁵⁰ Similarly, the spin diffusion length, which is used to represent the spin relaxation in the real space, is also controlled by the inhomogeneous broadening and the scattering, with the relative strength of them dividing the system into the weak/strong scattering regime. At 120 K, the electron-LO-phonon scattering is very weak and falls into the weak scattering regime. Therefore the diffusion length decreases with the scattering. But at 300 K, the scattering becomes stronger. Our results indicate the system is near the transition regime between the strong and weak scattering and therefore the changes are marginal by adding new scattering.

C. Temperature and well width dependence of spin diffusion

In Fig. 3 the steady-state spin-resolved electron density N_σ and the incoherently summed spin coherence ρ are plotted as functions of position x at different temperatures $T = 120, 200$ and 300 K for QW with $a = 7.5$ nm. In the calculation only the intrinsic scattering is included. One finds from the figure that the spin precession period increases with the temperature. This is because the period is around $|\Omega_0^{-1}| = [m^* \gamma |\langle k_y^2 \rangle - (\pi/a)^2|]^{-1}$. With the increase of temperature, $\langle k_y^2 \rangle$ increases. Consequently the period of the spacial spin oscillation becomes longer.

The spin diffusion length decreases with the temperature. This is understood that with the increase of temperature, both the inhomogeneous broadening and the scattering increase. In the weak scattering regime, this increase leads to a faster spin R/D. Nevertheless, the temperature dependence of the spin diffusion length is very mild compared to the temperature dependence of the spin precession period.

We further study the well-width dependence of the spin diffusion in the steady state in Fig. 4, with only the intrinsic scattering included at $T = 120$ K. One finds from the

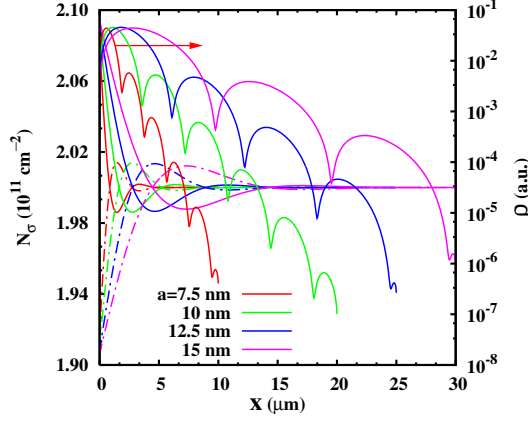


FIG. 4: (Color online) N_σ and ρ vs. the position x at different quantum well widths $a = 7.5, 10, 12.5$, and 15 nm (with $L = 10, 20, 25$ and 30 μm respectively) at $T = 120$ K. The solid curves stand for N_\uparrow and ρ , and the dash-dotted ones represent N_\downarrow . Note the scale of the incoherently summed spin coherence is on the right hand side of the figure.

figure that both the spin oscillation period and the spin diffusion length increase markedly with the well width. This is consistent with the spin R/D time in the time domain⁴⁷ and is understood due to the decrease of the Dresselhaus spin-orbit coupling Eq. (4) in which the linear term is proportional to $1/a^2$.

D. Magnetic field dependence of spin diffusion

We investigate the effect of magnetic field on the spin R/D in the steady state spin diffusion. It has been pointed out by Weng and Wu that the magnetic field plays a different role in spin diffusion/transport from the time-domain spin precession in the spacial uniform case.²¹ In the spin precession in the time domain, the magnetic field alone without the DP term will not cause any spin R/D due to the absence of inhomogeneous broadening.⁴⁵ Whereas in spin diffusion/transport, as the inhomogeneous broadening is caused by $\Omega_{\mathbf{k}}$ which reads $m^*g\mu_B B/k_x$ in the absence of the DP term and still provides an inhomogeneous broadening leading to the spin R/D.²¹ Furthermore, from Eq. (19) one finds that the inhomogeneous broadening caused by the applied magnetic field depends on the direction of the magnetic field when it is combined with the inhomogeneous broadening caused by the effective magnetic field $m^*\mathbf{h}(\mathbf{k})/k_x$. Therefore different direction of the magnetic field yields different spin diffusion length.

We reveal the magnetic field effect on the steady-state spin diffusion by plotting in Fig. 5 the spin diffusion length L_d and the spin oscillation period L_0 , fitted from the calculated spin polarization along the z -direction by $\Delta N_z(x)/N_e = C \exp(-x/L_d) \cos(2\pi x/L_0 + \phi)$, as function of the applied magnetic field at $T = 120$ K. The direction of the magnetic field is either vertical (along

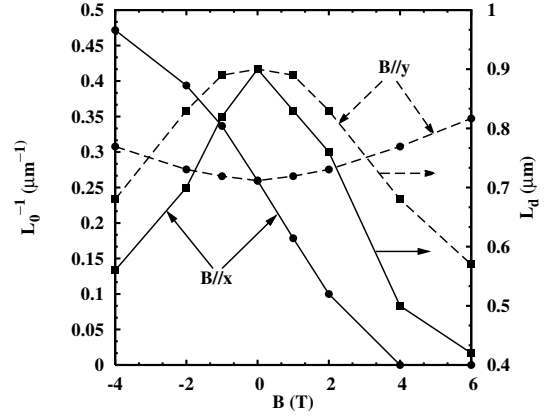


FIG. 5: Inverse of the period of the spin oscillation L_0^{-1} (curves with \bullet) and the spin diffusion length L_d (curves with \blacksquare) vs. the external magnetic field B which is applied either vertical ($\parallel y$, dashed curves) or parallel ($\parallel x$, solid curves) to the diffusion direction. $T = 120$ K and $N_i = 0$. The dashed curves are for the vertical magnetic field and the solid curves are for the parallel one. Note the scale of the diffusion length L_d is on the right hand side of the figure.

the y -axis) or parallel (along the x -axis) to the diffusion direction.

One finds from the figure that the magnetic field leads to additional spin R/D and therefore the spin diffusion length decreases with the magnetic field, regardless of the direction of the magnetic field. However, it is interesting to see that the spin diffusion length has different symmetry when the magnetic field is vertical or parallel to the spin diffusion direction: When \mathbf{B} is parallel to the y -axis, $L_d(B) = L_d(-B)$; However, when \mathbf{B} is parallel to the x -axis, $L_d(B) \neq L_d(-B)$. This can be understood from the fact that the density matrices from the kinetic spin Bloch equations (8) have the symmetry $\rho_{k_x, k_y, k_z}(B) = \rho_{k_x, -k_y, k_z}(-B)$ when \mathbf{B} is along the y -axis. This symmetry is broken if \mathbf{B} is along the x -axis.

Differing from the magnetic field dependence of the spin diffusion length, the spin oscillation period L_0 decreases monotonically with the vertical magnetic field, regardless the direction of the field. However L_0 increases with the parallel magnetic field when the field is along the diffusion direction and less than 4 T (the spin precession disappears when the field is larger than 4 T) but L_0 increases with the magnetic field when it is anti-parallel to the diffusion direction. The spacial period is determined by $\Omega_0 + m^*g\mu_B \mathbf{B}/\langle k_x \rangle$ with Ω_0 being along the x -axis. $\langle k_x \rangle$ represents the average of k_x due to the spin gradient and can be roughly estimated by $\langle k_x \rangle = \sum_{\mathbf{k}} k_x \Delta f_{\mathbf{k}} / \sum_{\mathbf{k}} \Delta f_{\mathbf{k}}$, which is a positive value due to the presence of the spin gradient. For the vertical magnetic field, Ω_0 and $\mathbf{B}/\langle k_x \rangle$ are perpendicular to each other, so the magnitude of the spin oscillation period is determined by $[\sqrt{(m^*g\mu_B \mathbf{B})^2 / \langle k_x \rangle^2 + \Omega_0^2}]^{-1}$ which always decreases with the magnetic field. However, for the parallel one, these two vectors are in the same direc-

tion and the period is determined by $|\gamma(\langle k_y^2 \rangle - \langle k_z^2 \rangle) + g\mu_B B / \langle k_x \rangle|^{-1}$. So the period increases with the magnetic field. Moreover, it is interesting to see that when $B \sim 4$ T, $|\gamma(\langle k_y^2 \rangle - \langle k_z^2 \rangle) + g\mu_B B / \langle k_x \rangle| \sim 0$ and further increasing of the magnetic field does not lead to any spin oscillation due to the too large inhomogeneous broadening caused by the magnetic field.

E. Electric field dependence of spin diffusion

We now turn to study the electric field effect on spin transport. An external electric field is applied along the x -axis. When the electric field is large enough, the spin transport is then in the hot-electron regime. It has been shown in our previous investigation^{48,72} in the spacial homogeneous case that the spin precession in the time domain is markedly affected by the electric field. Especially an effective magnetic field $\gamma v_d \pi^2 / (a^2 m^*)$, which is proportional to the electric field, is induced by the electric field combined with the DP term due to the center-of-mass drift velocity $v_d = \mu E$ (and hence $k_x = v_d / m^*$) driven by the electric field, with μ representing the mobility. This effective magnetic field leads to a spin precession in the absence of any magnetic field and the precession frequency changes with the variation of the electric field.⁴⁸ One may therefore expect that now in spin transport, the spacial spin oscillation period is also proportional to the electric field. This is *not* the case as again k_x in the spin diffusion terms, *i.e.*, the third terms in Eq. (8), plays an important role in the spin diffusion/transport and consequently the spacial oscillation period Ω_0^{-1} is *independent* on k_x . Therefore, in spin transport the electric field cannot induce an additional spacial spin precession. It is further expected that in the steady state, $\langle k_x \rangle$ is now determined by both the drift velocity and the spin gradient. Therefore, if the electric field $E_x > 0$ (< 0), $\langle k_x \rangle$ is reduced (enhanced) by the electric field and the spin diffusion length depends on the direction of the electric field.

In Fig. 6 the spin density ΔN in the steady state is plotted against the position x at different electric fields $E = 0.5, 0, -0.5$ and -1 kV/cm with only the intrinsic scattering included at $T = 120$ K. It is seen from the figure that the spin oscillation period is almost unchanged when the electric field varies from -1 kV/cm to 0.5 kV/cm. This is consistent with the latest experimental observation in bulk system.¹⁵ It is further noticed from the figure that the spin diffusion length is markedly affected by the electric field. To reveal this effect, the spin diffusion length is plotted as function of electric field in the same figure. One finds when the electric field varies from -1 kV/cm to $+1$ kV/cm, the spin diffusion length decreases monotonically. This can be easily understood from the fact that when an electric field is applied along $-x$ -direction ($+x$ -direction), the drift velocity caused by the electric field is along the x -direction ($-x$ -direction), which enhances (cancels) the velocity driven by the spin

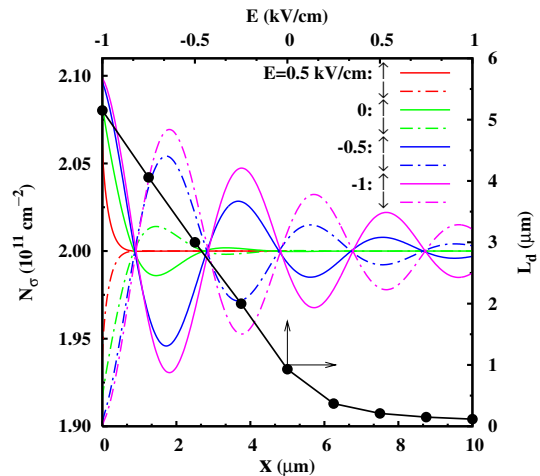


FIG. 6: (Color online) Spin-resolved electron density N_σ vs. position x at different electric field $E = 0.5, 0, -0.5$ and -1 kV/cm and the spin diffusion length L_d against the electric field E at $T = 120$ K. $N_i = 0$. It is noted that although x is plotted up to $10 \mu\text{m}$, $L = 25 \mu\text{m}$ when $E = -1.0$ and -0.75 kV/cm; $20 \mu\text{m}$ when $E = -0.5$ and -0.25 kV/cm; $10 \mu\text{m}$ when $E = 0$; and $5 \mu\text{m}$ when $E = 0.5, 0.75$ and 1.0 kV/cm. Note the scales of the spin diffusion length are on the top and the right hand side of the figure.

gradient. Therefore, $\langle k_x \rangle$ is increased (reduced) and the inhomogeneous broadening is decreased (enhanced). A longer (shorter) spin diffusion length is then observed.

IV. SUMMARY

In summary, we have performed a theoretical investigation on the spin diffusion/transport in n -type GaAs QWs at high temperatures (≥ 120 K) by setting up and numerically solving the kinetic spin Bloch equations together with the Poisson equation, with all the scattering explicitly included. A new numerical scheme is developed which can solve the kinetic equations with high accuracy and speed.

The spin R/D mechanism in the spin diffusion/transport is due to the inhomogeneous broadening, combined with the spin conserving scattering. Differing from the spin precession in the spacial uniform system where the inhomogeneous broadening is caused only by the momentum-dependent effective magnetic field due to the SOC, in spin diffusion/transport, the inhomogeneous broadening is caused additionally by the momentum dependence in the spin diffusion rate and therefore even the magnetic field alone can lead to spin R/D. Due to the joint effects from the momentum-dependence in the diffusion rate and the momentum dependence in the Dresselhaus effective magnetic field, there are spin oscillations along the spin diffusion even in the absence of the external magnetic field. The period of these spacial spin oscillations can be affected by the temperature, the well width and the electron density, but is independent

on the external electric field. It increases when an additional scattering is added or the temperature/the well width is increased. Moreover, it is shown that when the scattering is strong enough, the spin oscillations of electrons at different momentum \mathbf{k} show the *same* period. In fact, the intrinsic scattering, *i.e.*, the electron-electron and the electron-LO-phonon scattering is already strong enough to lead to this effect. This indicates that during the spin diffusion, there is no interference-induced spin dephasing and $L_p = L_p^*$.

It is shown that the Coulomb scattering makes marked contribution to the spin R/D in the spin diffusion/transport. It is especially important in the hot-electron case as it provides the important mechanism of thermalization. The scattering, the temperature, the QW width, the magnetic field and the electric field dependence of the spin diffusion length and the spacial spin oscillation period are explored in detail. It is shown that in the weak scattering regime, the spin diffusion length decreases if a new scattering is added into the system, while in the strong scattering regime, it increases. In the temperature regime we are interested in, the spin diffusion length decreases with the temperature. Moreover, it increases with the increase of the QW width as the inhomogeneous broadening decreases with the well width but decreases with the external magnetic field as the later adds a new inhomogeneous broadening into the system. The external electric field can effectively prolong or suppress the spin diffusion length depending on whether the electric field is antiparallel or parallel to the spin diffusion direction. We believe this investigation is useful for the

understanding of the spin transport as well as the design of the spintronic device.

Acknowledgments

This work was supported by the Natural Science Foundation of China under Grant Nos. 90303012 and 10574120, the Natural Science Foundation of Anhui Province under Grant No. 050460203, the National Basic Research Program of China under Grant No. 2006CB922005, the Knowledge Innovation Project of Chinese Academy of Sciences and SRFDP. The authors acknowledge valuable discussions with M. Q. Weng and M. P. Zhang.

APPENDIX A: NUMERICAL SCHEME FOR KINETIC SPIN BLOCH EQUATIONS

The kinetic spin Bloch equations Eq. (8) can be rewritten as:

$$\frac{\partial}{\partial t}\rho_{\mathbf{k}}(x, t) + \frac{k_x}{m^*} \frac{\partial}{\partial x}\rho_{\mathbf{k}}(x, t) = G_{\mathbf{k}}[x, t] \quad (\text{A1})$$

with $G_{\mathbf{k}}[x, t] = \left. \frac{\partial \rho_{\mathbf{k}}(x, t)}{\partial t} \right|_{\text{dr}} + \left. \frac{\partial \rho_{\mathbf{k}}(x, t)}{\partial t} \right|_{\text{coh}} + \left. \frac{\partial \rho_{\mathbf{k}}(x, t)}{\partial t} \right|_{\text{scat}}$. The discretization of the time and spatial derivatives in Eq. (A1) reads

$$\begin{aligned} & \frac{1}{2} \left[\frac{\rho_{\mathbf{k}}(x, t + \Delta t) - \rho_{\mathbf{k}}(x, t)}{\Delta t} + \frac{\rho_{\mathbf{k}}(x + \Delta x, t + \Delta t) - \rho_{\mathbf{k}}(x + \Delta x, t)}{\Delta t} \right] + \frac{k_x}{m^*} \frac{\rho_{\mathbf{k}}(x + \Delta x, t + \Delta t) - \rho_{\mathbf{k}}(x, t + \Delta t)}{\Delta x} \\ &= \frac{1}{2} (G_{\mathbf{k}}[x, t] + G_{\mathbf{k}}[x + \Delta x, t]) . \end{aligned} \quad (\text{A2})$$

For $k_x > 0$, the electron is propagated from its left positions to the right ones. Therefore, from Eq. (A2), the iterative format is

$$\rho_{\mathbf{k}}(x + \Delta x, t + \Delta t) = -\frac{1-r}{1+r} \rho_{\mathbf{k}}(x, t + \Delta t) + \frac{1}{1+r} (\rho_{\mathbf{k}}(x, t) + \rho_{\mathbf{k}}(x + \Delta x, t)) + \frac{\Delta t}{1+r} (G_{\mathbf{k}}[x, t] + G_{\mathbf{k}}[x + \Delta x, t]) . (\text{A3})$$

For $k_x < 0$, the electron state is propagated from its right positions and the iterative format is then

$$\rho_{\mathbf{k}}(x, t + \Delta t) = -\frac{1-r}{1+r} \rho_{\mathbf{k}}(x + \Delta x, t + \Delta t) + \frac{1}{1+r} (\rho_{\mathbf{k}}(x + \Delta x, t) + \rho_{\mathbf{k}}(x, t)) + \frac{\Delta t}{1+r} (G_{\mathbf{k}}[x, t] + G_{\mathbf{k}}[x + \Delta x, t]) . (\text{A4})$$

In these equations $r = \frac{2|k_x|\Delta t}{m^*\Delta x}$.

We truncate the spacial variable x from 0 to L . At the left edge, the boundary conditions are given only for the states with $k_x > 0$ and at the right edge only for those with $k_x < 0$. Note the state with $k_x = 0$ does not contribute to the diffusion process but contributes to

the local source term $G_{\mathbf{k}}[x, t]$. With the combined effects of the spin-flip terms and the scattering terms, the spin signal decays when it diffuses into the QW in the scale of the diffusion length L_d . When $L \gg L_d$, one can study the spin injection properties.

The computation is carried out in a parallel manner in the “Beowulf” cluster. For a typical calculation with the partitions 16×18 grid points in the (k, θ) -space and 400

points in the real space, it takes about 7 hours for the system to evolve to 300 ps with a time step of 0.023 ps by 6-node AMD Athlon XP3000+CPU’s.

-
- * Author to whom all correspondence should be addressed; Electronic address: mwwu@ustc.edu.cn.
- † Mailing Address
- ¹ *Semiconductor Spintronics and Quantum Computation*, ed. by D. D. Awschalom, D. Loss, and N. Samarth (Springer-Verlag, Berlin, 2002); I. Žutić, J. Fabian, and S. Das Sarma, *Rev. Mod. Phys.* **76**, 323 (2004).
 - ² S. A. Wolf, D. D. Awschalom, R. A. Buhrman, J. M. Daughton, S. von Molnár, M. L. Roukes, A. Y. Chtchelkanova, and D. M. Treger, *Science* **294**, 1488 (2001).
 - ³ J. M. Kikkawa, I. P. Smorchkova, N. Samarth, and D. D. Awschalom, *Science* **277**, 1284 (1997).
 - ⁴ J. M. Kikkawa and D. D. Awschalom, *Nature (London)* **397**, 139 (1999).
 - ⁵ J. M. Kikkawa and D. D. Awschalom, *Phys. Rev. Lett.* **80**, 4313 (1998).
 - ⁶ H. Ohno, *Science* **281**, 951 (1998).
 - ⁷ T. Adachi, Y. Ohno, F. Matsukura, and H. Ohno, *Physica E* **10**, 36 (2001).
 - ⁸ J. M. Kikkawa and D. D. Awschalom, *Science* **287**, 473 (2000); *ibid.* **281**, 656 (2000).
 - ⁹ Y. Ohno, D. K. Young, B. Beschoten, F. Matsukura, H. Ohno, and D. D. Awschalom, *Nature (London)* **402**, 790 (1999).
 - ¹⁰ R. Fiederling, M. Keim, G. Reuscher, W. Ossau, G. Schmidt, A. Waag, and L.W. Molenkamp, *Nature (London)* **402**, 787 (1999).
 - ¹¹ M. A. Brand, A. Malinowski, O. Z. Karimov, P. A. Marsden, R. T. Harley, A. J. Shields, D. Sanvitto, D. A. Ritchie, and M. Y. Simmons, *Phys. Rev. Lett.* **89**, 236601 (2002).
 - ¹² J. Stephens, J. Berezovsky, J. P. McGuire, L. J. Sham, A. C. Gossard, and D. D. Awschalom, *Phys. Rev. Lett.* **93**, 097602 (2004).
 - ¹³ J. Strand, B. D. Schultz, A. F. Isakovic, C. J. Palmstrøm, and P. A. Crowell, *Phys. Rev. Lett.* **91**, 036602 (2003).
 - ¹⁴ G. Schmidt, C. Gould, P. Grabs, A. M. Lunde, G. Richter, A. Slobodskyy, and L. W. Molenkamp, *Phys. Rev. Lett.* **92**, 226602 (2004).
 - ¹⁵ M. Beck, C. Metzner, S. Malzer, and G. H. Döhler, *Europhys. Lett.* **75**, 597 (2006).
 - ¹⁶ S. A. Crooker and D. L. Smith, *Phys. Rev. Lett.* **94**, 236601 (2005).
 - ¹⁷ M. Johnson, *Phys. Rev. B* **58**, 9635 (1998).
 - ¹⁸ Y. Takahashi, K. Shizume, and N. Masuhara, *Phys. Rev. B* **60**, 4856 (1999).
 - ¹⁹ M. Osofsky, *J. Supercond.* **13**, 209 (2000).
 - ²⁰ M. E. Flatté and J. M. Byers, *Phys. Rev. Lett.* **84**, 4220 (2000).
 - ²¹ M. Q. Weng and M. W. Wu, *Phys. Rev. B* **66**, 235109 (2002).
 - ²² J. Fabian, I. Žutić and S. Das Sarma, *Phys. Rev. B* **66**, 165301 (2002).
 - ²³ Z. G. Yu and M. E. Flatté, *Phys. Rev. B* **66**, 201202(R) (2002); *ibid.* **66**, 235302 (2002).
 - ²⁴ I. Martin, *Phys. Rev. B* **67**, 014421 (2003).
 - ²⁵ M. Q. Weng and M. W. Wu, *J. Appl. Phys.* **93**, 410 (2003).
 - ²⁶ Y. Qi and S. Zhang, *Phys. Rev. B* **67**, 052407 (2003).
 - ²⁷ M. Q. Weng, M. W. Wu, and Q. W. Shi, *Phys. Rev. B* **69**, 125310 (2004).
 - ²⁸ L. Jiang, M. Q. Weng, M. W. Wu, and J. L. Cheng, *J. Appl. Phys.* **98**, 113702 (2005).
 - ²⁹ S. Saikin, M. Shen, M.-C. Cheng, and V. Privman, *J. Appl. Phys.* **94**, 1769 (2003).
 - ³⁰ V. V. Osipov and A. M. Bratkovsky, *Phys. Rev. B* **70**, 205312 (2004).
 - ³¹ Y. Y. Wang and M. W. Wu, *Phys. Rev. B* **72**, 153301 (2005).
 - ³² M. Hruška, Š. Kos, S. A. Crooker, A. Saxena, and D. L. Smith, *Phys. Rev. B* **73**, 075306 (2005).
 - ³³ S. Pramanik, S. Bandyopadhyay, and M. Cahay, *Phys. Rev. B* **73**, 125309 (2006).
 - ³⁴ H. Dery, L. Cywiński, and L. J. Sham, *Phys. Rev. B* **73**, 041306(R) (2006).
 - ³⁵ D. Csontos and S. E. Ulloa, *Physica E* **32**, 412 (2006); *Phys. Rev. B* **74**, 155207 (2006).
 - ³⁶ X. Jiang, R. Wang, R. M. Shelby, R. M. Macfarlane, S. R. Bank, J. S. Harris, and S. S. P. Parkin, *Phys. Rev. Lett.* **94**, 056601 (2005).
 - ³⁷ E. I. Rashba, *Phys. Rev. B* **62**, R16276 (2000).
 - ³⁸ *Optical Orientation*, edited by F. Meier and B.P. Zakharchenya (North-Holland, Amsterdam, 1984).
 - ³⁹ A. G. Aronov, G. E. Pikus, and A. N. Titkov, *Zh. Éksp. Teor. Fiz.* **84**, 1170 (1983) [*Sov. Phys. JETP* **57**, 680 (1983)].
 - ⁴⁰ Yu. V. Pershin and V. Privman, *Phys. Rev. B* **69**, 73310 (2004).
 - ⁴¹ S. Saikin, *J. Phys.: Cond. Matt.* **16**, 5071 (2004).
 - ⁴² E. G. Mishchenko and B. I. Halperin, *Phys. Rev. B* **68**, 045317 (2003).
 - ⁴³ D. Schmeltzer, A. Saxena, A. R. Bishop, and D. L. Smith, *Phys. Rev. B* **68**, 195317 (2003).
 - ⁴⁴ O. Bleibaum, *Phys. Rev. B* **71**, 195329 (2005).
 - ⁴⁵ M. W. Wu and C. Z. Ning, *Eur. Phys. J. B* **18**, 373 (2000).
 - ⁴⁶ M. W. Wu, *J. Phys. Soc. Jpn.* **70**, 2195 (2001).
 - ⁴⁷ M. Q. Weng and M. W. Wu, *Phys. Rev. B* **68**, 075312 (2003).
 - ⁴⁸ M. Q. Weng, M. W. Wu, and L. Jiang, *Phys. Rev. B* **69**, 245320 (2004).
 - ⁴⁹ J. Zhou, J. L. Cheng, and M. W. Wu, *Phys. Rev. B* **75**, 045305 (2007).
 - ⁵⁰ C. Lü, J. L. Cheng, and M. W. Wu, *Phys. Rev. B* **73**, 125314 (2006).
 - ⁵¹ L. Allen and J. H. Eberly, *Optical Resonance and Two-level Atoms* (Dover, New York, 1975).
 - ⁵² B. H. Floyd and Y. L. Le Coz, *J. Appl. Phys.* **76**, 7889 (1996).
 - ⁵³ Y. L. Le Coz, Ph.D thesis, Massachusetts Institute of Technology, 1988.
 - ⁵⁴ J. A. Carrillo, I. M. Gamba, A. Majorana, C.-W. Shu, *J. of Comput. Phys.* **184**, 498 (2003).
 - ⁵⁵ H. Haug and A.P. Jauho, *Quantum Kinetics in Transport and Optics of Semiconductors* (Springer, Berlin, 1996).

- ⁵⁶ M. I. D'yakonov and V. I. Perel', Zh. Éksp. Teor. Fiz. **60**, 1954 (1971) [Sov. Phys.-JETP **33**, 1053 (1971)].
- ⁵⁷ G. Dresselhaus, Phys. Rev. **100**, 580 (1955).
- ⁵⁸ Y. A. Bychkov and E. Rashba, Sov. Phys. JETP Lett. **39**, 78 (1984); Y. A. Bychkov and E. Rashba, Pis'ma Zh. Eksp. Teor. Fiz. **39**, No. 2, 66 (1984).
- ⁵⁹ B. G. Streetman and S. Banerjee, *Solid State Electronic Devices* (Prentice Hall, Englewood Cliffs, NJ, 2000), Eq. (5.14); K. Tomizawa, *Numerical Simulation of Submicron Semiconductor Devices* (Artech House, Boston, 1993), Eq. (4.16); M. V. Fischetti and S. E. Laux, *DAMOCLES Theoretical Manual*, (IBM Corporation, New York, 1995) Document No. 0.2, Eq. (3.34).
- ⁶⁰ J. L. Cheng and M. W. Wu, J. Appl. Phys. **99**, 083704 (2006).
- ⁶¹ M. M. Glazov and E. L. Ivchenko, Pis'ma Zh. Éksp. Teor. Fiz. **75**, 476 (2002) [JETP Lett. **75**, 403 (2002)].
- ⁶² E. Ya. Sherman, Appl. Phys. Lett. **82**, 209 (2003).
- ⁶³ M. W. Wu and H. Metiu, Phys. Rev. B **61**, 2945 (2000).
- ⁶⁴ T. Kuhn and F. Rossi, Phys. Rev. Lett. **69**, 977 (1992).
- ⁶⁵ P. Y. Yu and Manuel Cardona, *Fundamentals of Semiconductors* (Springer, Berlin, 2003).
- ⁶⁶ E. M. conwell and M. O. Vassel, IEEE trans. ED-**13**, 22-27 (1966).
- ⁶⁷ Gerald D. Mahan, *Polar Semiconductors*, ed. J. T. Devreese (North-Holland, Amsterdam, 1972); Gerald D. Mahan, *Many-Particle Physics* (Plenum press, New York, 1981).
- ⁶⁸ We also checked the division with $(N, M) = (32, 34)$ and 800 grids in the real space and obtained the almost identical results. So the accuracy of the numerical calculation is high enough. The reason that for such a rough \mathbf{k} -mesh the results are converged lies on two facts: one is that, as shown in Sec. III(A), all the density matrix elements in the \mathbf{k} -space are in the same phase; the other is that the system is almost in the non-degenerate regime. Therefore the spin polarization in the k -space is extended to a very large energy scale and is therefore very smooth.
- ⁶⁹ *Semiconductors*, Landolt-Börnstein, New Series, Vol. 17a, ed. by O. Madelung (Springer-Verlag, Berlin, 1987).
- ⁷⁰ C. Lü, J. L. Cheng, M. W. Wu, and I. C. da Cunha Lima, Phys. Lett. A (2007), doi:10.1016/j.physleta.2007.02.030.
- ⁷¹ A. M. Tyryshkin, S. A. Lyon, W. Jantsch, and F. Schäffler, Phys. Rev. Lett. **94**, 126802 (2005).
- ⁷² L. Jiang and M. W. Wu, Phys. Rev. B **71**, 033311 (2005).